Title

The effect of 2,3,5,6-tetrafluoro-7,7,8,8-tetracyanoquinodimethane charge transfer dopants on the conformation and aggregation of poly(3-hexylthiophene)

Journal

Journal of Materials Chemistry C, 1(36)

ISSN

2050-7526

Authors

Gao, Jian
Roehling, John D
Li, Yongle
et al.

Publication Date

2013

DOI

10.1039/c3tc31047g

Peer reviewed

Journal of Materials Chemistry C

Materials for optical and electronic devices

www.rsc.org/MaterialsC

Volume 1 | Number 36 | 28 September 2013 | Pages 5597–5808

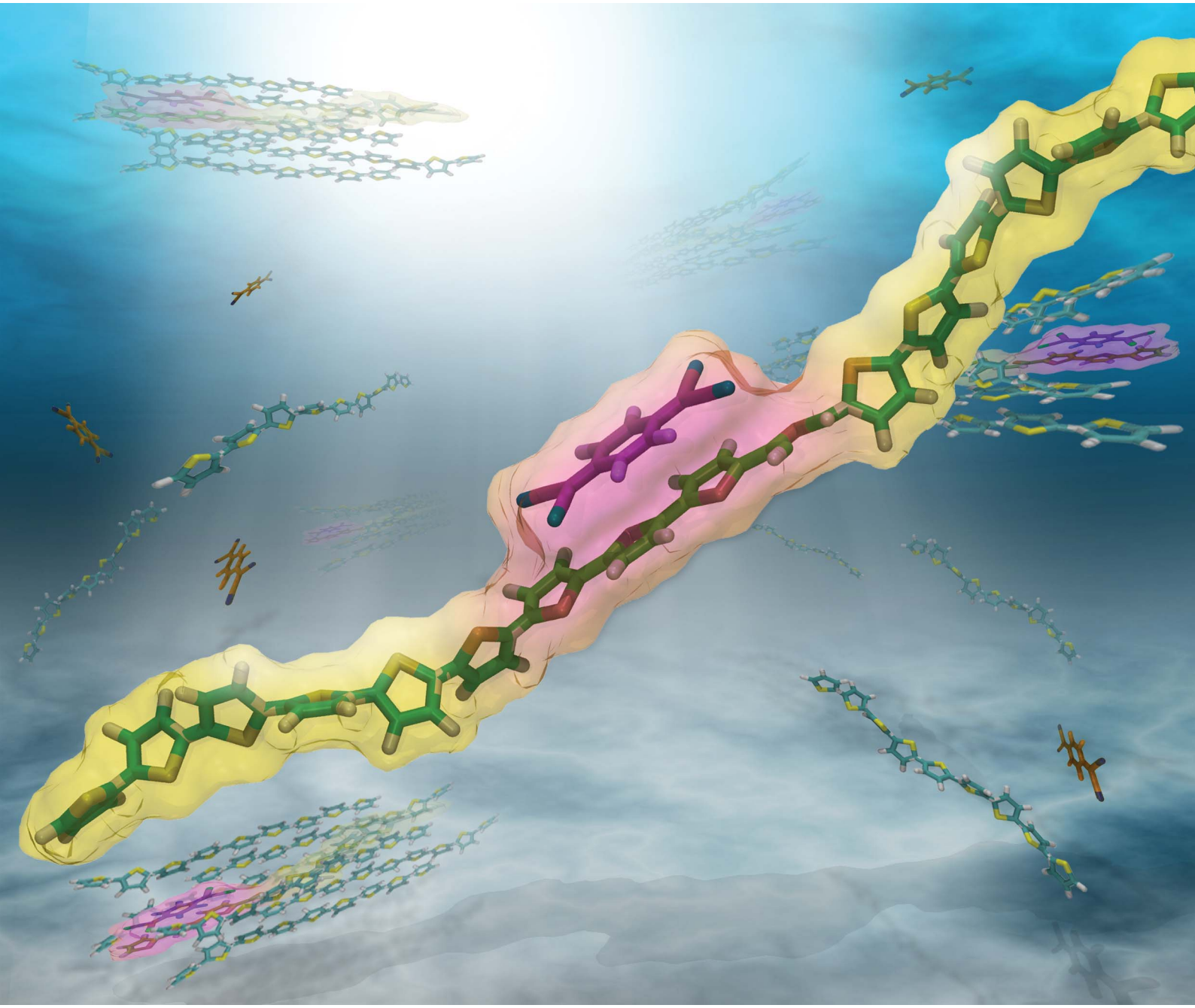

ISSN 2050-7526

RSC Publishing

PAPER

John K. Grey *et al.*

The effect of 2,3,5,6-tetrafluoro-7,7,8,8-tetracyanoquinodimethane charge transfer dopants on the conformation and aggregation of poly(3-hexylthiophene)

2050-7526(2013)1:36;1-A

Journal of Materials Chemistry C

RSC Publishing

PAPER

View Article Online
View Journal | View Issue

Cite this: J. Mater. Chem. C, 2013, 1, 5638

The effect of 2,3,5,6-tetrafluoro-7,7,8,8-tetracyanoquinodimethane charge transfer dopants on the conformation and aggregation of poly(3-hexylthiophene)†

Jian Gao,[a] John D. Roehling,[b] Yongle Li,[a] Hua Guo,[a] Adam J. Moulé[b] and John K. Grey*[a]

Received 1st June 2013
Accepted 20th July 2013

DOI: 10.1039/c3tc31047g

www.rsc.org/MaterialsC

The effect of the strong electron acceptor, 2,3,5,6-tetrafluoro-7,7,8,8-tetracyanoquinodimethane (F_4-TCNQ), on poly(3-hexylthiophene) (P3HT) aggregates is studied. F_4-TCNQ is commonly used as a dopant for P3HT, however, relatively little is currently known about its effect on polymer conformation and packing in the presence of fullerenes. Resonance Raman and optical spectra of pristine P3HT or blends with [6,6]-phenyl-C_{61}-butyric acid methyl ester (PCBM) doped with F_4-TCNQ up to ~10% w/w show a loss of pristine-type P3HT aggregates with increasing dopant concentration. Complexed P3HT chains possess greater backbone planarity due to hole injection which is corroborated from density functional theory (DFT) calculations of oligothiophene surrogates and F_4-TCNQ. Morphologies of doped P3HT/PCBM systems are characterized using scanning transmission electron microscopy (STEM) with electron energy loss spectroscopy (EELS) detection and images reveal mixed clusters of P3HT/F_4-TCNQ fibril-like domains that increase in size with dopant loading. The apparent preference of F_4-TCNQ for P3HT aggregates is attributed to efficient charge separation stemming owing to the more polarizable nature of chains comprising the aggregate π-stack.

Introduction

Charge transfer dopants are effective for tuning electronic properties of organic semiconductors.[1,2] Doping of polymer/fullerene solar cell blends has resulted in significant improvements in power conversion efficiencies arising from better charge generation and transport.[3,4] While electrical properties have been well-studied and mechanistic aspects of charge transfer doping are emerging,[1,2,5,6] the understanding of changes in the polymer structure and morphology has lagged behind. This aspect is important in crystalline polymers where charge transport efficiency depends on the ability of the polymer to form well-packed domains (*i.e.*, aggregates). Moreover, fullerenes limit the ability of the polymer to aggregate, which may have unforeseen impacts on material performance.

We study the effect of doping using the strong electron acceptor, 2,3,5,6-tetrafluoro-7,7,8,8-tetracyanoquinodimethane (F_4-TCNQ), with a regio-regular poly(3-hexylthiophene) (P3HT) system with blends of [6,6]-phenyl-C_{61}-butyric acid methyl ester (PCBM). Various spectroscopic techniques and chemical mapping *via* electron energy loss spectroscopy (EELS) in a scanning transmission electron microscope (STEM) are used to ascertain the effect of doping on P3HT aggregation and overall morphology.

Efficient doping occurs when the LUMO of the acceptor is deeper than the HOMO of the polymer donor and a hole is injected onto the former.[1,5,7] Doping is generally believed to be a two step process for organic semiconductors where the donor is first ionized followed by dissociation of the charge transfer pair. Charge transfer doping is readily achieved in P3HT (HOMO ~ 5.0 eV) using the F_4-TCNQ acceptor with its LUMO lying at ~5.2 eV.[7–12] Formation of a charge transfer complex in P3HT/F_4-TCNQ systems was predicted by Aziz *et al.*[13] but the manner in which the complex dissociates into free charges is still actively debated.[5,6] Pingel and Neher recently reported that integer charge transfer occurs upon contact of P3HT with F_4-TCNQ as opposed to the more commonly accepted partial (hybrid) charge transfer description.[6] These authors show that a large fraction of charges remain bound thus explaining the lower than expected amounts of free charge carriers.[7]

[a]Department of Chemistry and Chemical Biology, University of New Mexico, Albuquerque, NM 87131, USA. E-mail: jkgrey@unm.edu; Fax: +1 505 277 2609; Tel: +1 505 277 1658

[b]Department of Chemical Engineering and Materials Science, University of California, Davis, CA 95616, USA. E-mail: amoule@ucdavis.edu; Tel: +1 530 754 8669

† Electronic supplementary information (ESI) available: Optical absorption spectra of P3HT and P3HT/PCBM blends with varying F_4-TCNQ, absorption and emission spectra of F_4-TCNQ doped P3HT nanofibres and simulated Raman spectra of (oligothiophene)$_4$/F_4-TCNQ complexes. See DOI: 10.1039/c3tc31047g

Doping P3HT with F_4-TCNQ has recently been used in solar cell applications and large improvements in device power conversion efficiency are possible. Most notably, improvements in the power conversion efficiency >1% have been obtained for the prototypical P3HT/PCBM blend for small amounts of F_4-TCNQ (<3%).[12] This improvement has been attributed to the increase in intrinsic carriers that modifies the effective Fermi level.[12] Enhanced charge percolation by stabilization of separated charges (increased permittivity) and increasing charge generation pathways thereby suppressing charge recombination have also been proposed.[5]

In P3HT/PCBM blends, the current view is that the volume fraction of aggregated P3HT chains increases due to the presence of F_4-TCNQ.[12] Duong *et al.* recently performed X-ray scattering studies on P3HT/F_4-TCNQ and showed compelling evidence for two different concentration dependent mixed phases.[14] These authors also confirmed that P3HT/F_4-TCNQ interactions are decided in the solution phase prior to thin film deposition, which is especially important since polymer conformation and aggregation are affected by solvent–solute interactions. Theoretical simulations have proved to be useful in exposing the nature of charge transfer interactions and a partial charge transfer of ~0.5 e^- was recently predicted between an oligothiophene and F_4-TCNQ.[15] However, further work is required to determine how dopants interact with the distinct morphological forms of P3HT (*i.e.*, amorphous and aggregated regions) which are regulated by the PCBM content as well as processing conditions.

We measure resonance Raman and optical spectra of P3HT and P3HT/PCBM blend thin films doped with varying amounts of F_4-TCNQ that help expose the nature of interactions between P3HT aggregates and dopants. We find that the amounts of pristine type P3HT aggregates decrease with increased dopant loading but complexed P3HT chains are more planar relative to their pristine state. This charge transfer induced planarity enhancement is apparent at low dopant loading (<10%) and gives rise to a greater J-aggregate character in optical spectra where high intrachain order reduces interchain exciton coupling.[16,17] We speculate that F_4-TCNQ dopants interact with dangling or looping chains on the periphery of nascent P3HT aggregates according to the integer charge transfer description. Subsequent charge separation (doping) is facilitated by the ordered π-stacked regions that permit intrachain charge delocalization. Hole injection into aggregated P3HT chains increases their backbone planarity and rigidity possibly from an increased quinoidal character.[18–21] DFT simulations using a similar model as reported in ref. 13 and 15 corroborate our experimental findings and we propose that the greater rigidity of the complexed P3HT chains destabilizes the pristine-type aggregate π-stacks leading to the previously proposed mixed phase possessing different packing characteristics.[14] STEM images with EELS detection show that the doped P3HT chains tend to cluster together leading to increased phase segregation in the presence of PCBM.

Experimental section

Sample preparation

Electronic grade, regio-regular poly-3-hexylthiophene (P3HT, $M_w \approx 50\,000$–$70\,000$ g mol^{-1}), [6,6]-phenyl-C_{61}-butyric acid methyl ester (PCBM) and 2,3,5,6-tetrafluoro-7,7,8,8-tetracyanoquinodimethane (F_4-TCNQ) were purchased from Aldrich and used without further purification. Materials were dissolved in anhydrous chlorobenzene (CB) at a concentration of 10 mg mL^{-1} (P3HT and PCBM) and 1 mg mL^{-1} (F_4-TCNQ) and stirred for ~12 h in a dry nitrogen environment. Solutions were filtered using a 0.2 μm filter (Whatman) to remove any undissolved solids and spun-cast onto clean glass coverslips. F_4-TCNQ was added to pristine P3HT and P3HT/PCBM blend (1 : 1 w/w) solutions by addition of F_4-TCNQ solutions to achieve 0, 1, 3, 4.8, and 9.1% w/w (dopant to polymer weight ratio) doping concentrations. The largest loading in pristine P3HT samples corresponds to equal amounts of polymer and dopant by weight (*i.e.*, 50%). In PCBM blends, the weight ratio of P3HT and PCBM is kept constant and the amount of F_4-TCNQ is varied up to a maximum value of ~33% (*i.e.*, equal amounts of each component). However, we emphasize lower amounts of dopants more commonly encountered in optoelectronic applications (*i.e.*, <10%). Thermal annealing treatments of thin films were applied by heating samples on a hot plate at 130 °C for 20 min in a nitrogen environment. P3HT nanofibres (NFs) displaying an H- or J-type aggregate character were fabricated using self-assembly methods described previously.[22] F_4-TCNQ was added to solution suspensions of NFs to determine the stability of the structures to charge transfer doping.

Spectroscopy, microscopy and simulations

Optical absorption spectra of solution and thin film samples were recorded on a UV/vis spectrometer (Varian). Photoluminescence (PL) and Raman spectra were acquired using a microscope-based spectrometer described in detail previously.[23] Thin film samples were placed in an inert gas flow cell to avoid photodegradation and were excited using the 488 nm line of an argon ion laser with excitation intensities of ~10^3 (PL) and ~10^4 (Raman) W cm^{-2}. Samples were raster scanned during continuous spectral acquisition and averaged. For the STEM/EELS imaging samples, P3HT of ~40 000 g mol^{-1} was used to increase the visibility of fibril-like structures. Solutions of P3HT/PCBM (1 : 1 w/w) were mixed with 0, 0.5, 2, and 5% w/w of F_4-TCNQ in chlorobenzene. These solutions were then cast onto a glass substrate coated with poly(3,4-ethylenedioxythiophene):poly(styrenesulfonate) (PEDOT:PSS) and annealed on a hotplate at 150 °C for 5 minutes. The films were then floated off the substrate and collected with a TEM grid. Images were collected in an aberration corrected JEOL 2100F microscope using a Gatan Imaging Filter (GIF) and the DigitalMicrograph software package. Spectrum images (SI) were obtained using a pixel size of ~4.5 nm. Sulfur maps were calculated from the SI using a power-law background subtraction and a 40 eV energy window beginning at 180 eV. Density functional theory (DFT) calculations on charge transfer complexes were carried out using the hybrid B3LYP functional. A four-member unsubstituted thiophene oligomer, $(thiophene)_4$, was used to model P3HT. For F_4-TCNQ, $(thiophene)_4$, and their complexes, the standard 6-311++G** basis set was used. A sandwich structure involving one $(thiophene)_4$ and two F_4-TCNQ molecules was also simulated

at the B3LYP/6-311+G* level that may represent possible complex structures encountered at high dopant loadings. The structures were first optimized, followed by the calculation of the Raman spectra. All calculations were performed using the Gaussian 09 suite.[24]

Results and discussion

Optical spectroscopy

This paper is primarily concerned with understanding the nature of the interaction of the dopant with crystalline and amorphous P3HT species. The relative amounts of each are regulated by PCBM acceptors[25] and processing conditions to help determine whether F_4-TCNQ dopants exhibit preferential interactions towards either form. We focus on dopant loadings commonly encountered in solar cell device applications (*i.e.*, <10%) which typically have a limited P3HT aggregate content.

Optical spectroscopy is an excellent tool to assess not only the amount of P3HT aggregates in various environments but also the type and strength of aggregate exciton coupling.[26,27] Fig. 1 shows absorption and PL spectra of pristine P3HT (A and B) and P3HT/PCBM blend (C and D) thin films with varying amounts of F_4-TCNQ. Previous optical spectroscopy lineshape analyses demonstrate that P3HT aggregates comprise ~50% or greater of the total P3HT chains in pristine films,[26,27] which is reduced substantially when PCBM is added. Absorption and PL 0–0/0–1 vibronic intensity ratios of the characteristic P3HT aggregate lineshapes show gradual increases upon addition of F_4-TCNQ up to 10%. Absorption and PL electronic origin energies (E_{0-0}) slightly red- and blue-shift, respectively, in this doping range causing a reduction in the Stokes shift. The greater sensitivity of PL to the presence of a dopant is expected because PL occurs from minority low energy sites at the bottom of energy funnels corresponding to aggregates. These trends are highlighted in Fig. 2 for both pristine P3HT (A) and P3HT/PCBM blends (B). As F_4-TCNQ content increases, signal-to-noise ratios decrease indicating a reduction in pristine-type P3HT. At F_4-TCNQ concentrations greater than 10%, the characteristic aggregate and amorphous absorption lineshapes diminish and transitions from the anion form of F_4-TCNQ[6,14] become dominant (see insets of Fig. 1A and C).

We now consider P3HT/PCBM blends doped with F_4-TCNQ to understand how F_4-TCNQ affects P3HT when it is mostly in its amorphous or, unaggregated, form. Fig. 1C and D present optical spectra of these doped blends that show similar trends as pristine P3HT films albeit larger linewidths due to greater disorder and fewer aggregates absorbing/emitting. The effect of F_4-TCNQ is more pronounced in PCBM blends suggesting that fullerenes accentuate the ground state charge transfer interaction between P3HT and F_4-TCNQ. We speculate that this effect appears from the smaller amounts of aggregates present in the PCBM blends. PL spectra of doped blends show nearly quantitative quenching when F_4-TCNQ loadings are larger than 3% that are consistent with the lower aggregate content. Importantly, there is no change in the vibronic interval (~1450 cm^{-1}) in either pristine or blend samples, demonstrating that changes in lineshapes are not due to self-absorption or artefacts.

A particularly noteworthy feature of optical spectra in Fig. 1 is the increase in 0–0/0–1 vibronic intensity ratios with the F_4-TCNQ content. PL spectra of pristine P3HT films show ~30% increase of the 0–0/0–1 ratios at 5% F_4-TCNQ doping but the amount of change is comparatively smaller for P3HT/PCBM blends. The increase of 0–0/0–1 vibronic ratios is consistent with increased J-aggregate character of P3HT chains meaning greater intrachain order or, planarity between monomers.[17] The fact that the aggregate portion of optical lineshapes is most affected indicates a stronger interaction with F_4-TCNQ. The observed transition to the J-aggregate character requires a significant enhancement in P3HT planarity which could be

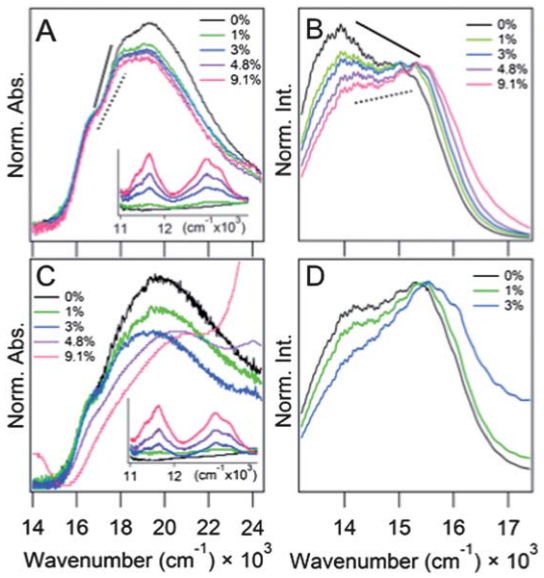

Fig. 1 Absorption and PL spectra for (A and B) P3HT films and (C and D) P3HT/PCBM blend films with F_4-TCNQ doping (w/w%), respectively. Spectra were normalized at their 0–0 maxima. Sloping lines in (A) and (B) are included as a guide for the eye for tracking vibronic intensities with the F_4-TCNQ content.

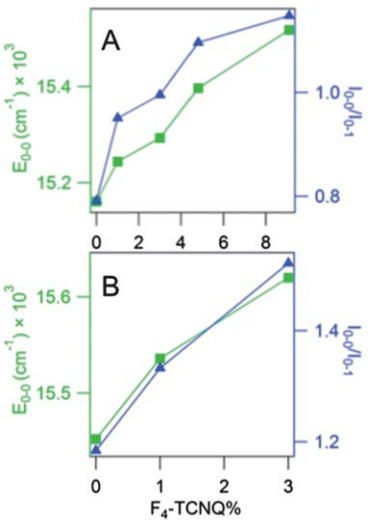

Fig. 2 Peak positions of 0–0 emission (green) and 0–0/0–1 intensity ratios (blue) for (A) P3HT films and (B) P3HT/PCBM blend films with F_4-TCNQ doping.

realized by injection of a hole carrier probably resulting in greater quinoidal character. This distortion increases chain rigidity and planarity[28] which was observed in previous redox doping and spectro-electrochemistry of polythiophene derivatives.[29,30] Although our optical spectra suggest that the intra-chain order increases in P3HT chains (for low doping amounts), it is not clear how the amounts of aggregated or unaggregated P3HT chains are affected.

Unfortunately, a detailed lineshape analysis of optical spectra using accepted models, such as the weakly coupled exciton theory developed by Spano and co-workers,[26,27] is complicated by the increased broadening and lower signal-to-noise ratios of the P3HT transitions with doping.

Raman spectroscopy

We instead turn to resonance Raman spectroscopy which overcomes issues with overlapping lineshapes, *etc.*, typically encountered in optical spectroscopy of conjugated polymers. This technique can be used for assessing the aggregate content[23] in addition to extracting excited state structural properties (*i.e.*, vibrational displacements) and dynamics.[31,32] Fig. 3 shows resonance Raman spectra of pristine P3HT and P3HT/PCBM blends with varying F_4-TCNQ contents using 488 nm excitation. This wavelength probes both aggregated and unaggregated P3HT chains nearly equally and the dominant C=C symmetric stretch of P3HT (~1450–1470 cm^{-1}) can be used to determine the relative amounts of each form as well as changes in the structure with doping.

It is first important to note that Raman spectra show resolved overtone transitions (0–*n*, $n > 1$) of up to two harmonics in the dominant P3HT C=C mode. Overtones are nearly integer multiples of the C=C fundamental demonstrating that ground state potentials are not significantly distorted from an ideal harmonic oscillator description. We find noticeable changes in the intensities and frequencies of both fundamentals and overtones when the F_4-TCNQ content is varied, similar to our previous work on poly(phenylene-vinylene)–acceptor charge transfer complexes.[32] The appearance of overtones in doped P3HT systems offers new views into the effects of ground state charge transfer interactions on excited state structural displacements. This is perhaps best understood in the time-dependent framework of resonance Raman spectroscopy where the ground state vibrational wavefunction is projected up to the excited state by absorption of a photon and evolves in time.[33,34] The time-dependent wavepacket follows the path of steepest descent (*i.e.*, largest displaced high frequency modes) and samples the excited state potential surface followed by scattering back to a different ground state vibrational level where this information can be 'read out'. From Fig. 3, the changes in overtone intensities and lineshapes with F_4-TCNQ doping indicate new excited state potential energy landscapes.

Normally, disorder effects and increased number of displaced modes result in the disappearance of overtones. However, the persistence of these transitions with F_4-TCNQ loading up to 10% demonstrates that the new P3HT/F_4-TCNQ phase remains ordered as inferred from corresponding optical spectra. Although the excitation energy used to generate resonance Raman spectra in these samples primarily selects P3HT species, complications can arise from the presence of dopants. This feature makes it difficult to analyse Raman intensities with doping to extract quantitative excited state structural vibrational displacements and dynamics. Instead, we use these spectra in a qualitative fashion to understand the effect of dopant on changes in the ground and excited state structure with and without PCBM acceptors.

Increasing the F_4-TCNQ content in pristine P3HT films causes gradual broadening of C=C peaks (0–1 and 0–2) particularly toward the lower energy side of the band. Overtones first show increased intensity with addition of F_4-TCNQ up to ~3% followed by a gradual decrease with increased loading (>5%). Red-shifts of these C=C transitions point to increased conjugation lengths or, enhanced planarity. Comparison between pristine and blend doped thin film Raman spectra also show larger 0–2/0–1 ratios in blends consistent with larger structural displacements.‡ Relative overtone intensities initially increase for both sample types with F_4-TCNQ loading (up to ~3%) but then decrease with higher loadings (*i.e.*, >3%), similar to doped P3HT Raman spectra without PCBM. Closer inspection of the fundamental (0–1) and first overtone (0–2) region in PCBM blend film Raman spectra show significant changes when F_4-TCNQ doping increases past ~5%. New transitions emerge in both regions, revealing changes in packing as well as the backbone structure. The maxima of the C=C region also show

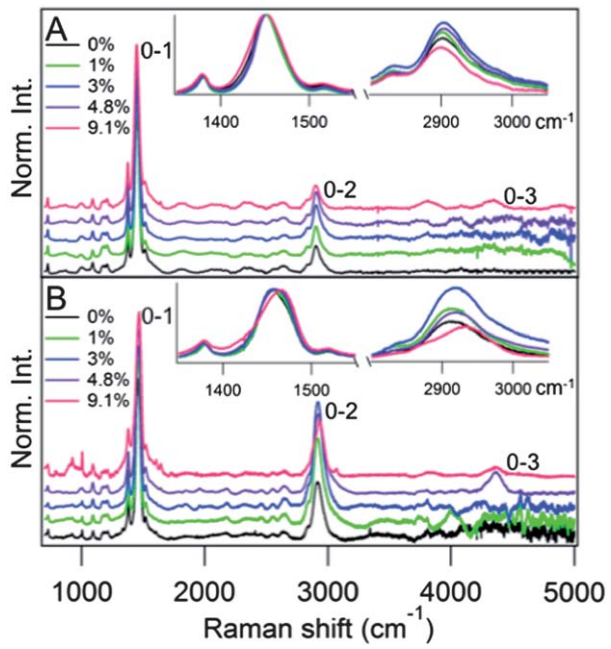

Fig. 3 Resonance Raman spectra for (A) P3HT films and (B) P3HT/PCBM films with F_4-TCNQ doping. Insets: blowups of the fundamental (0–1) and first overtone (0–2) regions of C=C symmetric stretching mode.

‡ Assuming that Raman scattering occurs from a single electronic state for both morphological forms (*i.e.*, aggregated and amorphous P3HT chains).

significant blue-shifts (~7 cm^{-1}) at ~10% F_4-TCNQ loading consistent with an increase of the unaggregated P3HT form.[23]

To better understand the manner in which F_4-TCNQ dopants interact with both P3HT forms, we use a simple two species model to decompose the Raman spectra.[26,27] For example, P3HT aggregates have their C=C maximum at ~1450 cm^{-1} whereas that of the unaggregated form appear at ~1470 cm^{-1}. The C=C fundamental band is fitted with two Lorentzian lineshapes corresponding to the two components of the P3HT C=C band and we emphasize on PCBM blend spectra since there are nearly equal amounts of both P3HT forms unlike pristine samples where more chains exist in the aggregated form. Fig. 4A shows the two component fits of the total P3HT C=C lineshape in PCBM blends with varying F_4-TCNQ amounts up to ~10%. Vertical lines are included as a guide for the eye that represent the centre frequencies of the aggregated and unaggregated component maxima in the absence of F_4-TCNQ corresponding to 1452 cm^{-1} and 1468 cm^{-1}, respectively. As the F_4-TCNQ content increases, the intensity of the aggregate component decreases indicating a loss of this species which is illustrated in Fig. 4B with plots of the intensity ratios of aggregated/unaggregated P3HT C=C contributions. Comparison of the centre frequencies of unaggregated C=C maxima show virtually no deviation with F_4-TCNQ content but the aggregate component exhibits a gradual red-shift of up to 5 cm^{-1} and increased broadening between 0% and 10% F_4-TCNQ loadings.

The ramifications of the decreased P3HT aggregate content in PCBM blends with doping are perhaps most apparent from recent studies involving pentacene doped with F_4-TCNQ.[35] Increased dopant loading resulted in a reduced crystalline domain size and increase of an amorphous pentacene phase,[35] similar to that observed here. Consequently, charge mobilities decreased due to this phase transition and the loss of P3HT aggregates past typical doping thresholds (~1–3%) may explain why the P3HT/PCBM solar cell performance decreases rapidly for higher dopant loadings.

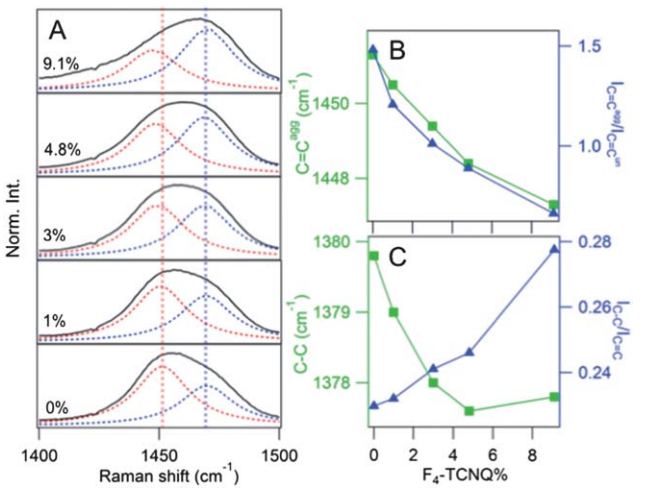

Fig. 4 (A) Fits of the P3HT C=C fundamental region of P3HT/PCBM films with varying F_4-TCNQ doping. (B) Aggregated C=C component centre frequency (green) and the Raman intensity ratios of aggregated to unaggregated components (blue) with F_4-TCNQ concentration. (C) P3HT C–C symmetric stretching Raman center frequency and C–C/C=C intensity ratios.

It is also useful to consider other prominent P3HT backbone modes that help illuminate changes in conformation and packing with doping. For example, the P3HT C–C symmetric stretch (~1370 cm^{-1}) is sensitive to chain planarity and comparison with the dominant C=C mode reveals correlations between backbone conformation and aggregation properties.[23,36] Fig. 4C plots the C–C frequency and C–C/C=C intensity ratios which show red-shifts and increases, respectively, with increased F_4-TCNQ loading. These trends are consistent with increased chain planarity and conjugation lengths (similar to those observed for the dominant C=C stretch).

Based on the trends outlined in Fig. 1–4, the overall pristine-type aggregate population decreases with the F_4-TCNQ content and a new phase corresponding to the complex is formed where P3HT chains possess increased planarity and, hence, increased J-aggregate character in optical spectra. Because the unaggregated component shows relative increases with increasing F_4-TCNQ loading up to 10% but no significant changes in frequency it is suggested that the dopant interacts preferentially with aggregated P3HT chains.

A possible explanation for the apparent preference of F_4-TCNQ for P3HT aggregates may lie in differences of oxidation potentials for both forms. For example, the measured HOMO level for mostly aggregated P3HT is ~5.0 eV and the LUMO of F_4-TCNQ is ~5.2 eV. Assuming that LUMO levels of aggregated and unaggregated forms are similar, the HOMO of the unaggregated form should be slightly deeper than that of the aggregated form by ~0.3 eV based on optical absorption energies.[11] This situation would make charge transfer slightly unfavourable for unaggregated P3HT whereas aggregates spontaneously undergo charge transfer with F_4-TCNQ prior to film deposition in solution. However, the current experiment cannot confirm whether or not the oxidation potentials of crystalline and amorphous P3HT forms are substantially different from one another.

We also explored whether the particular type of exciton coupling in the aggregate had an effect on doping efficiency. For example, variable F_4-TCNQ doping was performed on self-assembled P3HT NFs displaying either H- or J-type exciton coupling to verify if the intra- and interchain order of P3HT chains in the aggregate affect the nature of the interaction with the dopant. It was found that addition of F_4-TCNQ at a level of 5% leads to almost complete quenching of H-type PL and a small, but noticeable, change to J-type behaviour whereas the J-type NFs were quenched to ~50% of their original level with no change in lineshape (see ESI†). Because P3HT chains in J-type NFs are already highly planarized in the aggregate π-stack, charge transfer interactions with F_4-TCNQ probably only quench PL by reducing the amount of emitters due to polaron quenching.

It is also worthwhile to consider that a significant fraction of P3HT exists in an 'amorphous' region on the periphery of an aggregate as dangling or looping chains.[37] We expect that F_4-TCNQ probably interacts with these P3HT segments more readily due to the close-packed nature of the aggregate

crystalline region. Following integer charge transfer, the hole can delocalize along chains in the crystalline region thereby doping the polymer. At higher dopant loadings, the pristine aggregate structure becomes unstable due to increased backbone rigidity and charged nature of complexed chains, and fewer interaction sites are available. These effects lead to reductions in doping efficiency and appear exacerbated in blends where the amounts and sizes of aggregates are considerably smaller than pristine samples. We have begun preliminary studies on regio-regular and regio-random P3HT variants in solution to better understand the exact roles of aggregates in determining the doping efficiency but these results will have to be published in a future report.

STEM/EELS imaging

STEM imaging with EELS detection was performed on P3HT/PCBM films with varying F_4-TCNQ loadings to learn about the morphologies in doped samples when there are fewer aggregates present. Fig. 5 shows STEM/EELS maps with the relative densities of sulphur as the contrast agent. For an aggregated P3HT domain, the sulphur density should increase, and appear as a brighter region. In the regions of mixed amorphous P3HT and PCBM, the sulphur intensity decreases due to decreased sulphur density from interspersed PCBM.[38,39] However, if the PCBM content of the mixed domain decreased, the relative intensity of sulphur would likewise increase and be visible as a brighter region in the sulphur maps. P3HT fibrils can be discerned in all four films corresponding to aggregated P3HT. In the doped samples, fibrils appear to cluster as indicated by the increased sulphur intensity, which also increases with increasing F_4-TCNQ content. Comparison of carbon : sulphur ratio maps between undoped and doped samples shows that darker regions in Fig. 5 correspond to PCBM-rich areas (see ESI†). The increase in apparent phase separation in doped samples can simply be attributed to the electrostatic interactions between the charged P3HT chains (and dopants) and their surroundings. The P3HT/F_4-TCNQ mixed phase (*i.e.*, salt) is very polar making the local environment of the complexes less energetically favourable for PCBM to reside in.

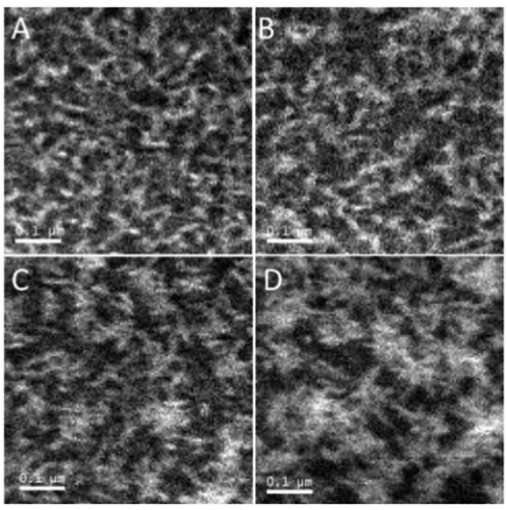

Fig. 5 Sulfur maps of P3HT/PCBM bulk films with (A) 0%, (B) 0.5%, (C) 2%, and (D) 5% F_4-TCNQ doping concentrations. Scale bar = 0.1 μm.

The images in Fig. 5 provide a more detailed view of the film morphology characteristics than scanned probe studies mainly owing to the roughness of the surface that may lead to artefacts. The tendency of complexed P3HT chains to cluster with increased dopant concentration gives the impression that aggregation is increasing. However, Raman spectra demonstrate that pristine-type P3HT aggregates decrease with dopant loading suggesting that these features in STEM/EELS images correspond to the newly mixed P3HT/F_4-TCNQ phase. Unfortunately, this technique cannot distinguish changes in packing and conformational aspects of P3HT but it does demonstrate that the fibril size is similar to pristine aggregates. However, these charged structures tend to cluster with increased dopant amounts making it difficult to reliably estimate their structural attributes. Using X-ray scattering techniques, Duong *et al.* demonstrated that this new mixed phase consisting of charged P3HT chains and F_4-TCNQ molecules possesses distinctly different packing characteristics than undoped P3HT aggregates.[14] We attempted to verify that the larger clumps of fibrils in doped films were in fact complexed P3HT, however, the chemical signal from the F_4-TCNQ (nitrogen or fluorine) was not strong enough to map its position. It is also important to stress that any TEM image is a projection through the volume, and three-dimensional information is lost. The reduced amounts of aggregates determined from Raman spectra of doped samples indicate that the quantifying aggregation content from these two-dimensional projections results in a poor indication of total aggregation.

The growth of a new mixed phase can shed light on the anomalous trends in Raman spectra in Fig. 3 where overtones show an initial increase in relative intensity followed by a decrease and broadening at higher dopant concentration. The fact that overtones persist in this new phase indicates that it is still well ordered, as confirmed by Duong *et al.*, but does not remain in the typical aggregate π-stack as originally proposed.[12,14] The increased broadening of these bands is also consistent with the broadening of the energetic distribution of charge transport sites with larger (>10%) F_4-TCNQ doping.[7]

Theoretical simulations

Based on the spectroscopic data in Fig. 1–4, P3HT aggregates appear to have a greater sensitivity to the presence of F_4-TCNQ than their unaggregated counterparts. While the dopant interacts with both the crystalline and amorphous regions of the aggregate, the former are better protected due to the close-packing of P3HT chains and we expect that F_4-TCNQ more readily complexes with dangling or looping chains (*i.e.*, amorphous region) on the periphery. Subsequent complex dissociation is realized by hole injection and intrachain delocalization into the nearby crystalline region. Raman spectra in particular indicate increased planarity of P3HT chains, which is consistent with the above hypothesis. Theoretical simulations are now

used to help confirm this proposed increase in planarity of the complexed P3HT chains from the experiment.

DFT calculations are performed on a model oligothiophene representing P3HT and F_4-TCNQ. A similar model was used previously by Aziz *et al.* and more recently by Zhu *et al.* to determine the amount of charge transfer between P3HT and F_4-TCNQ.[13,15] These authors vary the distance and orientation between the two molecules to assess the degree of charge transfer using calculated IR spectra as a predictive tool.[15] These studies reported changes in characteristic vibrational frequencies of F_4-TCNQ (*i.e.*, CN stretches) as a means to estimate the degree of charge transfer. Here, we wish to understand the effect of F_4-TCNQ interaction on a P3HT chain segment to determine if backbone planarity is significantly affected. Raman spectra of the resultant complexes are then simulated and compared to the experiment.

A thiophene oligomer with four monomer units, $(thiophene)_4$, is used to represent a P3HT segment that interacts with the dopant which is reasonable since the footprint of F_4-TCNQ spans a few thiophene monomer units. In addition, a sandwich type structure is considered where two F_4-TCNQ molecules interact with the $(thiophene)_4$ backbone. Although this structure is not expected at low to modest dopant concentrations (*i.e.*, <10%), it may emerge at higher concentrations. Fig. 6 shows the optimized $(thiophene)_4$ and F_4-TCNQ structures for the single complex (complex I) and the sandwich structure (complex II). Comparison of both structures reveals a larger $(thiophene)_4$–F_4-TCNQ separation for complex II over complex I (3.69 Å *vs.* 3.54 Å, respectively). More importantly, we notice large changes in the planarity of the $(thiophene)_4$ backbone depending on the nature of the complex interaction. Table 1 summarizes calculated dihedral angles for both complexes, which are defined in Scheme 1.

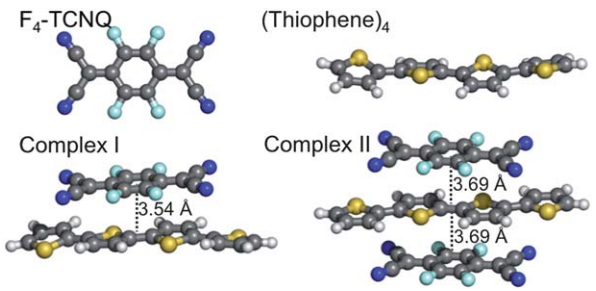

Fig. 6 Optimized geometries of F_4-TCNQ, $(thiophene)_4$, complex I and complex II.

Table 1 Dihedral angles of thiophene monomers from $(thiophene)_4$, complex I and complex II

Dihedral angle, ϕ	$(Thiophene)_4$	Complex I	Complex II
S–C–C–S	20.13	9.52	0.001
C_1=C–C=C_1	19.40	8.33	0.002
C_2–C–C–C_2	22.83	9.64	0
C_3–C–C–C_3	13.27	6.61	0

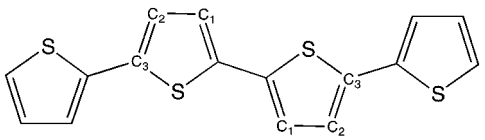

Scheme 1 Atomic definition for the $(thiophene)_4$ oligomer.

As shown in Fig. 6 and Table 1, the optimized $(thiophene)_4$ oligomer exists in a non-planar geometry but planarizes upon formation of a charge transfer complex with F_4-TCNQ, as evidenced by the smaller dihedral angle, ϕ. An additional F_4-TCNQ in the sandwich structure makes the oligomer even more planar presumably due to increased intermolecular electronic delocalization between the two acceptors and the oligomer backbone.

The amount of charge transferred in both configurations is estimated from calculated Mulliken populations with ~0.5 e^- transferred in complex I compared to ~0.2 e^- in complex II. The smaller amount of charge transferred in the latter is reasonable since charge is delocalized over two acceptors.

These results are consistent with experimental observations demonstrating increased P3HT backbone planarity upon interacting with F_4-TCNQ. Unfortunately, it was not possible at the level of theory used to simulate longer chains and assess the extent of charge delocalization.

Fig. 7 shows calculated frontier energy levels for complexes I and II. These energy levels are the result of intermolecular orbital mixing between the HOMO of $(thiophene)_4$ and the LUMO of F_4-TCNQ. It is clear from Fig. 7 that the HOMOs of the complexes allow a greater extent of electron delocalization, which is responsible for the planarization of $(thiophene)_4$. Comparison of HOMO–LUMO gaps for both complexes reveals a larger value for complex I (*i.e.*, 1.11 eV *vs.* 0.869 eV). Calculated Raman spectra for complexes I and II show red-shifts for the dominant C=C peak (see ESI†) similar to the experiment. However, experimental Raman spectra herein are generated on resonance with P3HT absorption transitions that likewise select

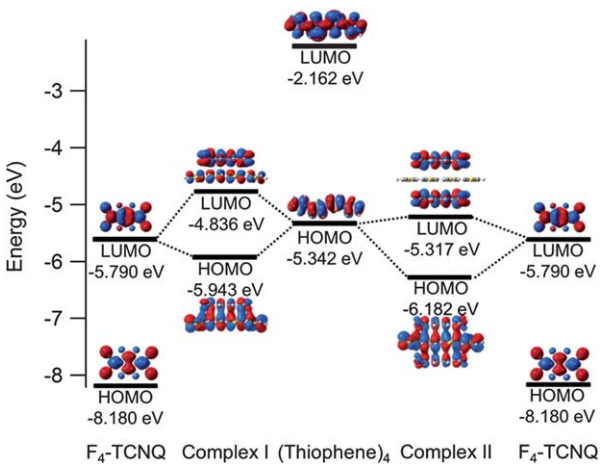

Fig. 7 HOMO and LUMO orbital energy levels and iso-surfaces (iso-value is 0.01) for F_4-TCNQ, $(thiophene)_4$ and their charge transfer complexes, complex I and complex II.

specific chromophores that more closely represent pristine P3HT. We are presently pursuing studies using off-resonance Raman scattering to further understand the nature of doping interactions. Nonetheless, DFT simulations do in fact corroborate trends in Raman and optical spectra indicating greater planarity upon doping.

The increase in P3HT chain planarity upon interacting with F_4-TCNQ may have some additional implications for charge transport and recombination. Conformational defects, such as kinks and bends, of the polymer backbone may act as shallow charge traps and lower short circuit current densities in solar cells. Enhanced polymer backbone planarity and rigidity should suppress this mechanism and therefore lead to improved device current densities.

Conclusions

We have demonstrated that P3HT aggregates appear to play a key role in determining doping efficiency using F_4-TCNQ acceptors and are susceptible to structural changes due to doping. A key finding from optical and Raman spectra was that doping increases the planarity of complexed P3HT chains. This was evident from the increased J-aggregate character in optical spectra, increased C–C/C=C intensities in Raman spectra as well as DFT simulations. The loss of pristine-type P3HT aggregates with increased dopant concentration arises from the increased rigidity of these charged chains. STEM/EELS images showed that the new P3HT/F_4-TCNQ phase consists of larger clusters of fibrils that probably result from the charged nature of this phase. The invariance of unaggregated P3HT segments with doping suggests that these species are not capable of delocalizing charge and thus difficult to effectively dope. Overall, ultimate doping efficiency appears to be determined by the ability of the P3HT to form aggregates, which can be seriously limited in PCBM blends. However, careful control of solution processing conditions may help mitigate these effects and increase doping efficiencies for solar cell applications.

Acknowledgements

J.K.G. acknowledges the National Science Foundation (CHE-0955242) for financial support. H.G. acknowledges the Defense Threat Reduction Agency (HDTRA1-11-1-0004) for partial support of this work. A.J.M. acknowledges Plextronics for supplying samples of P3HT.

Notes and references

1 K. Walzer, B. Maennig, M. Pfeiffer and K. Leo, *Chem. Rev.*, 2007, **107**, 1233–1271.
2 B. Luessem, M. Riede and K. Leo, *Phys. Status Solidi A*, 2013, **210**, 9–43.
3 K.-H. Yim, G. L. Whiting, C. E. Murphy, J. J. M. Halls, J. H. Burroughes, R. H. Friend and J.-S. Kim, *Adv. Mater.*, 2008, **20**, 3319–3324.
4 Y. Zhang, B. de Boer and P. W. M. Blom, *Adv. Funct. Mater.*, 2009, **19**, 1901–1905.
5 A. Mityashin, Y. Olivier, T. Van Regemorter, C. Rolin, S. Verlaak, N. G. Martinelli, D. Beljonne, J. Cornil, J. Genoe and P. Heremans, *Adv. Mater.*, 2012, **24**, 1535–1539.
6 P. Pingel and D. Neher, *Phys. Rev. B: Condens. Matter Mater. Phys.*, 2013, **87**, 115209.
7 P. Pingel, R. Schwarzl and D. Neher, *Appl. Phys. Lett.*, 2012, **100**, 143303.
8 Y. Zhang and P. W. M. Blom, *Appl. Phys. Lett.*, 2010, **97**, 083303.
9 X. Han, Z. Wu and B. Sun, *Org. Electron.*, 2013, **14**, 1116–1121.
10 H. Fujita, Y. Yuan and T. Michinobu, *J. Photopolym. Sci. Technol.*, 2011, **24**, 311–315.
11 J. Hu, K. W. Clark, R. Hayakawa, A.-P. Li and Y. Wakayama, *Langmuir*, 2013, **29**, 7266–7270.
12 A. Loiudice, A. Rizzo, M. Biasiucci and G. Gigli, *J. Phys. Chem. Lett.*, 2012, **3**, 1908–1915.
13 E. F. Aziz, A. Vollmer, S. Eisebitt, W. Eberhardt, P. Pingel, D. Neher and N. Koch, *Adv. Mater.*, 2007, **19**, 3257–3260.
14 D. T. Duong, C. Wang, E. Antono, M. F. Toney and A. Salleo, *Org. Electron.*, 2013, **14**, 1330–1336.
15 L. Zhu, E.-G. Kim, Y. Yi and J.-L. Brédas, *Chem. Mater.*, 2011, **23**, 5149–5159.
16 F. C. Spano, *Acc. Chem. Res.*, 2010, **43**, 429–439.
17 E. T. Niles, J. D. Roehling, H. Yamagata, A. J. Wise, F. C. Spano, A. J. Moule and J. K. Grey, *J. Phys. Chem. Lett.*, 2012, **3**, 259–263.
18 Y. Furukawa, *J. Phys. Chem.*, 1996, **100**, 15644–15653.
19 M. Lapkowski and A. Pron, *Synth. Met.*, 2000, **110**, 79–83.
20 J. Casado, M. Z. Zgierski, P. C. Ewbank, M. W. Burand, D. E. Janzen, K. R. Mann, T. M. Pappenfus, A. Berlin, E. Perez-Inestrosa, R. P. Ortiz and J. T. Lopez Navarrete, *J. Am. Chem. Soc.*, 2006, **128**, 10134–10144.
21 G. Louarn, M. Trznadel, J. P. Buisson, J. Laska, A. Pron, M. Lapkowski and S. Lefrant, *J. Phys. Chem.*, 1996, **100**, 12532–12539.
22 J. D. Roehling, I. Arslan and A. J. Moule, *J. Mater. Chem.*, 2012, **22**, 2498–2506.
23 Y. Gao and J. K. Grey, *J. Am. Chem. Soc.*, 2009, **131**, 9654–9662.
24 M. J. Frisch, H. B. Schlegel, G. E. Scuseria, M. A. Robb, J. R. Cheeseman, G. Scalmani, V. Barone, B. Mennucci, G. A. Petersson, H. Nakatsuji, M. Caricato, X. Li, H. P. Hratchian, A. F. Izmaylov, J. Bloino, G. Zheng, J. L. Sonnenberg, M. Hada, M. Ehara, K. Toyota, R. Fukuda, J. Hasegawa, M. Ishida, T. Nakajima, Y. Honda, O. Kitao, H. Nakai, T. Vreven, J. A. Montgomery, Jr, J. E. Peralta, F. Ogliaro, M. Bearpark, J. J. Heyd, E. Brothers, K. N. Kudin, V. N. Staroverov, R. Kobayashi, J. Normand, K. Raghavachari, A. Rendell, J. C. Burant, S. S. Iyengar, J. Tomasi, M. Cossi, N. Rega, J. M. Millam, M. Klene, J. E. Knox, J. B. Cross, V. Bakken, C. Adamo, J. Jaramillo, R. Gomperts, R. E. Stratmann, O. Yazyev, A. J. Austin, R. Cammi, C. Pomelli, J. W. Ochterski, R. L. Martin, K. Morokuma, V. G. Zakrzewski, G. A. Voth, P. Salvador, J. J. Dannenberg, S. Dapprich, A. D. Daniels,

Ö. Farkas, J. B. Foresman, J. V. Ortiz, J. Cioslowski and D. J. Fox, Gaussian Inc., 2009.
25 Y. Gao, T. P. Martin, E. T. Niles, A. J. Wise, A. K. Thomas and J. K. Grey, *J. Phys. Chem. C*, 2010, **114**, 15121–15128.
26 J. Clark, C. Silva, R. H. Friend and F. C. Spano, *Phys. Rev. Lett.*, 2007, **98**, 206406.
27 J. Clark, J.-F. Chang, F. C. Spano, R. H. Friend and C. Silva, *Appl. Phys. Lett.*, 2009, **94**, 163306.
28 E. Busby, E. C. Carroll, E. M. Chinn, L. Chang, A. J. Moulé and D. S. Larsen, *J. Phys. Chem. Lett.*, 2011, **2**, 2764–2769.
29 G. Louarn, M. Trznadel, J. P. Buisson, J. Laska, A. Pron, M. Lapkowski and S. Lefrant, *J. Phys. Chem.*, 1996, **100**, 12532–12539.
30 Y. Furukawa, M. Akimoto and I. Harada, *Synth. Met.*, 1987, **18**, 151–156.
31 A. B. Myers, *Acc. Chem. Res.*, 1997, **30**, 519–527.
32 A. J. Wise and J. K. Grey, *Phys. Chem. Chem. Phys.*, 2012, **14**, 11273–11276.
33 E. J. Heller, *Acc. Chem. Res.*, 1981, **14**, 368–375.
34 E. J. Heller, R. Sundberg and D. Tannor, *J. Phys. Chem.*, 1982, **86**, 1822–1833.
35 H. Kleemann, C. Schuenemann, A. A. Zakhidov, M. Riede, B. Luessem and K. Leo, *Org. Electron.*, 2012, **13**, 58–65.
36 W. C. Tsoi, D. T. James, J. S. Kim, P. G. Nicholson, C. E. Murphy, D. D. C. Bradley, J. Nelson and J.-S. Kim, *J. Am. Chem. Soc.*, 2011, **133**, 9834–9843.
37 T. Brinkmann, *Polym. Phys.*, 2011, **49**, 1218–1233.
38 B. A. Collins, E. Gann, L. Guignard, X. He, C. R. McNeill and H. Ade, *J. Phys. Chem. Lett.*, 2010, **1**, 3160–3166.
39 N. D. Treat, M. A. Brady, G. Smith, M. F. Toney, E. J. Kramer, C. J. Hawker and M. L. Chabinyc, *Adv. Energy Mater.*, 2010, **1**, 82–89.